ACS APPLIED MATERIALS & INTERFACES

www.acsami.org

Research Article

Adhesion Engineering in Polymer–Metal Comolded Joints with Biomimetic Polydopamine

Georgios Kafkopoulos, Clemens J. Padberg, Joost Duvigneau,* and G. Julius Vancso*

Cite This: *ACS Appl. Mater. Interfaces* 2021, 13, 19244–19253

Read Online

ACCESS | Metrics & More | Article Recommendations | Supporting Information

ABSTRACT: Joints that connect thermoplastic polymer matrices (TPMs) and metals, which are obtained by comolding, are of growing importance in numerous applications. The overall performance of these constructs is strongly impacted by the TPM–metal interfacial strength, which can be tuned by tailoring the surface chemistry of the metal prior to the comolding process. In the present work, a model TPM–metal system consisting of poly(methyl methacrylate) (PMMA) and titanium is used to prepare comolded joints. The interfacial adhesion is quantified by wire pullout experiments. Pullout tests prior to and following surface modification are performed and analyzed. Unmodified wires show poor interfacial strength, with a work of adhesion (G_a) value of 3.8 J m^{-2}. To enhance interfacial adhesion, a biomimetic polydopamine (PDA) layer is first deposited on titanium followed by a second layer of a poly(methyl methacrylate-*co*-methacrylic acid) (P(MMA-*co*-MAA)) copolymer prior to comolding. During processing, the MAA moieties of the copolymer thermally react with PDA, forming amide bonds, while MMA promotes the formation of secondary bonds and molecular interdigitation with the PMMA matrix. Control testing reveals that neither PDA nor the copolymer provides a substantial increase in adhesion. However, when used in combination, a significant increase in adhesion is detected. This observation indicates a pronounced synergistic effect between the two layers that strengthens the PMMA-titanium bonding. Enhanced adhesion is optimized by tuning the MMA-to-MAA ratio of the copolymer, which shows a maximum at a 24% MAA content and a greatly increased G_a value of 155 J m^{-2}; this value corresponds to a 40-fold increase. Further growth in the G_a values at higher MAA contents is hindered by the thermal cross-linking of MAA; MAA contents above 24% restrict the formation of secondary bonds and molecular interdigitation with the PMMA chains. Our results provide new design principles to produce thermoplastic–metal comolded joints with strong interfaces.

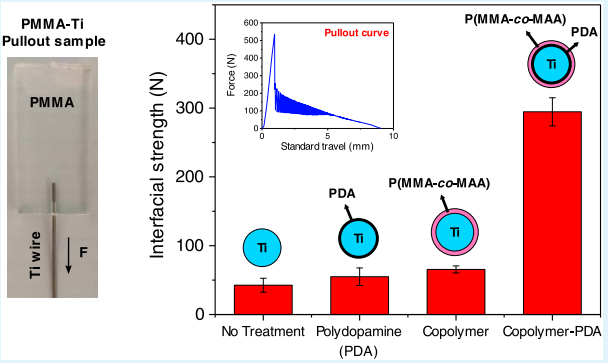

KEYWORDS: *polydopamine, coating, comolding, PMMA, titanium, polymer–metal adhesion, polymer–metal joint*

1. INTRODUCTION

Efficient comolding of thermoplastic polymer matrices (TPMs) with metals to form hybrid structures is of paramount importance for various technologies, including those in energy, electronics, automotive, and aerospace applications.[1−4] Regarding TPMs, comolding usually refers to a process in which a metal is joined with a molten polymer matrix, followed by cooling, to achieve the formation of a polymer–metal joint. In such processes, inferior adhesion between the polymer matrix and metal often results in a weak interfacial strength. In addition, failure at the interface is enhanced by thermal stresses generated by the mismatch of the respective thermal expansion ratios, further reducing the overall performance of the joint.[5]

Strategies to enhance the TPM–metal interfacial strength can be divided into three categories on the basis of the length scale at which they function, including the macro-, micro-, and nanoscales. At the macroscale, the main focus is the design of the overall geometry of the joint.[6] Issues at the microscale are concerned with the effect of roughness in terms of mechanical interlocking and the interfacial contact area.[7] At the nanoscale, molecular interactions prevail[8] and chemical modifications can be employed to couple poorly interacting materials.[9] Regarding challenges at the nanoscale, reports have focused on using conventional coupling agents, such as silanes, to promote adhesion in comolded joints.[10−12] We believe that if progress is to be made toward designing and forming high-performance joints, new approaches are needed, particularly at the nanoscale. Biomimetic adhesives based on poly(dopamine) (PDA) have recently been studied due to their capacity to provide the required increase in interfacial adhesion.[13,14] To this end, the present work focuses on the molecular interactions that occur at

Received: January 19, 2021
Accepted: April 1, 2021
Published: April 13, 2021

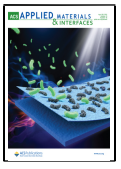

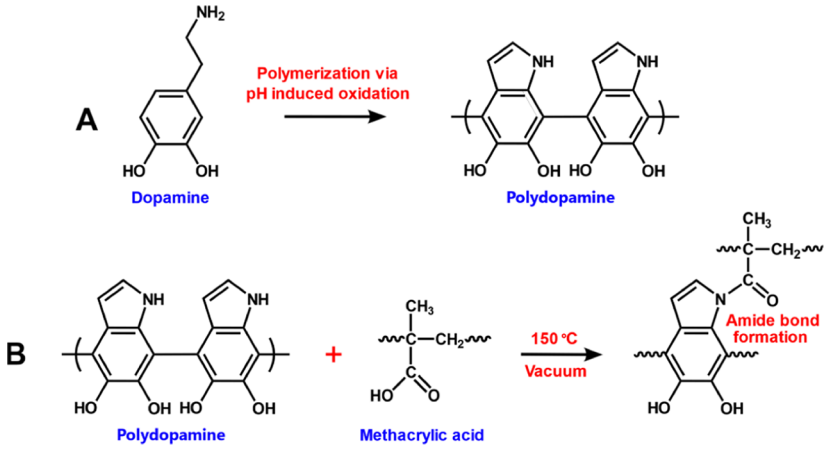

Figure 1. Polydopamine formation via the pH-induced oxidation of dopamine (A) and amide bond formation between polydopamine and methacrylic acid (B).[24,25]

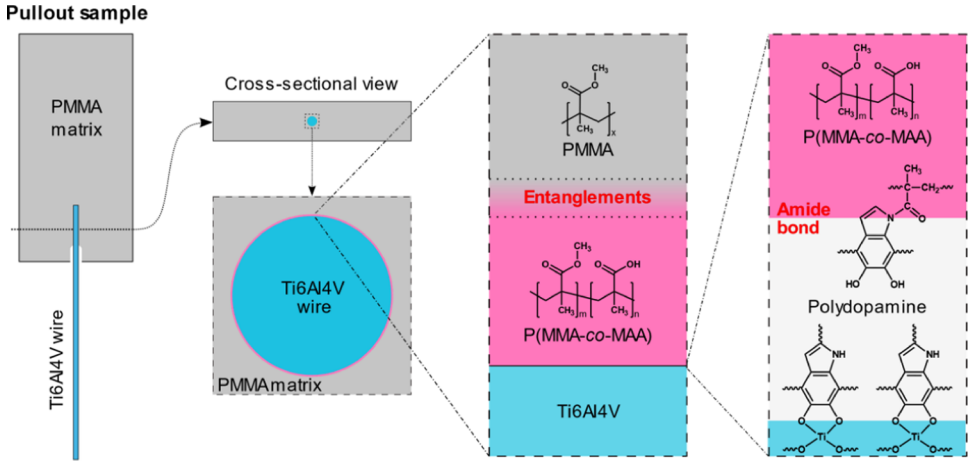

Figure 2. Schematic representation of a wire pullout sample and the applied surface modifications located on different length scales. The dimensions of the pullout sample and coating are scaled.

the TPM−metal oxide interface and how they can be engineered by employing PDA.

Metal oxides and polymeric species usually bond via acid−base interactions occurring between donor/acceptor groups that are present in the polymer chain and at the oxide surface.[15] When the polymer chain architecture does not promote molecular interactions, surface modifications are required to enhance adhesion.[11] As mentioned, in this study, we utilize PDA[16−20] for improving adhesion at the interface.

Inspired by the strong mussel adhesion in harsh marine environments, Messersmith and co-workers[21] polymerized dopamine under alkaline conditions (Figure 1A) and observed the formation of a PDA layer on the surface of virtually any material immersed in the aqueous solution during the polymerization process. The PDA film that is formed is known to participate in three types of reactions.[13] In the case of metal oxide surfaces, using TiO_2 (rutile) as a substrate, density functional theory calculations have shown that the dopamine molecules orient nearly perpendicular to the surface, with the hydroxyl groups coordinated toward TiO_2.[22,23] This result bolsters the interaction strength and enhances adhesion.

In this study, we focus on the reaction of PDA with carboxylic acid[24,25] to form amide bonds (Figure 1B). We also note that the thermal treatment of PDA at 150 °C improves the cohesiveness of the PDA layer,[26] which is a good indication of the thermal stability of this PDA layer at the comolding temperatures required for thermoplastics (i.e., 150−300 °C). The ability of PDA to strongly bind to various substrates, in combination with its postmodification possibilities and expected thermal stability,[13,27] shows that it has high potential to improve adhesion in TPM−metal comolded joints.

Since it was first synthesized,[21] PDA has been applied as a coupling agent in different nanocomposite systems obtained by thermal processing, with some systems showing improvements in their mechanical performance.[28−36] However, in these studies, the effect of PDA on interfacial adhesion was not quantitatively elucidated. Therefore, it remains unclear whether the observed improvements originate from enhanced interfacial adhesion or from other factors (e.g., an increase in the frictional interaction of filler with the matrix). In addition, there have been no reports on the application of PDA for improving adhesion in TPM−metal comolded joints. Thus, the goal of the present study is to apply PDA on the metal surface of a comolded TPM−metal system that is known to exhibit poor interfacial strength, evaluate the effect of PDA by quantifying the work of adhesion, and maximize the interfacial strength by utilizing the reactivity of PDA.

To evaluate adhesion, fiber pullout experiments were employed due to their proven and successful application in quantifying the interfacial work of adhesion of a variety of

https://doi.org/10.1021/acsami.1c01070
ACS Appl. Mater. Interfaces 2021, 13, 19244−19253

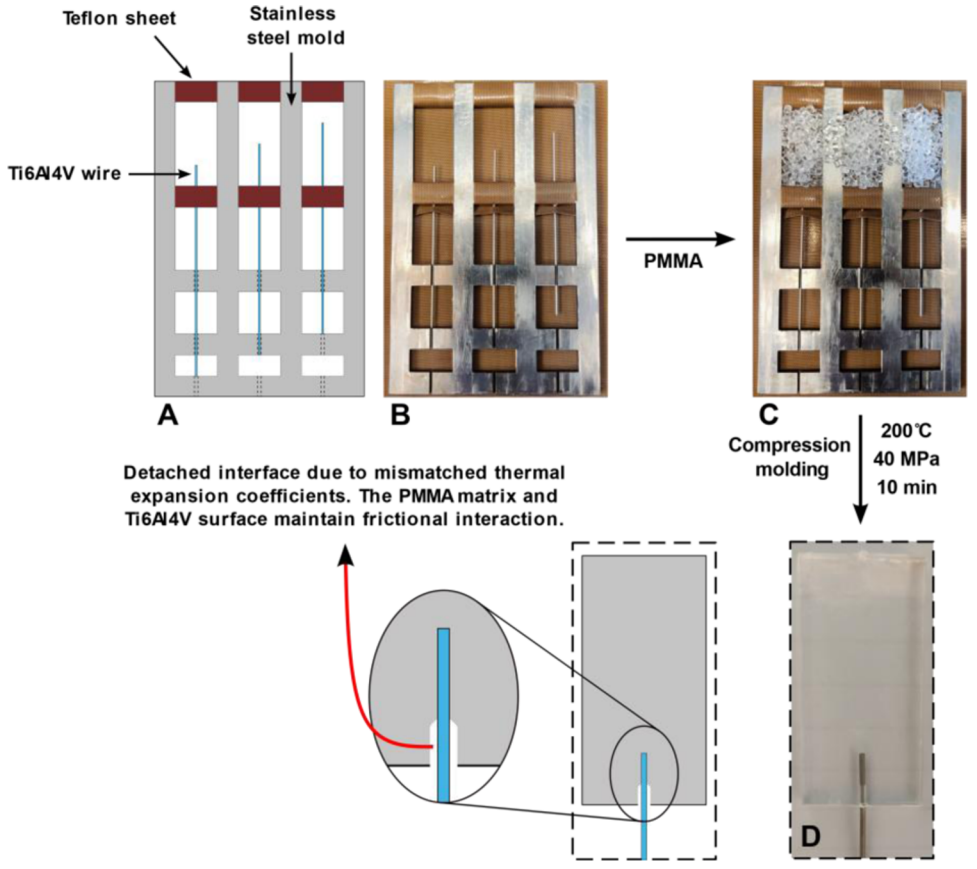

Figure 3. Schematic depicting the mold design and Ti6Al4V wire placement (A) and an actual image of the same. (B) Mold filled with PMMA pellets before the comolding process (C) and a photograph of a pullout specimen (D).

materials.[37−43] Comolded specimens were prepared using titanium grade 5 (Ti6Al4V) wires and poly(methyl methacrylate) (PMMA) as a model system. Ti6Al4V was chosen for its commercial relevance, whereas PMMA is known to exhibit poor adhesion with metals, thus providing plenty of room for adhesion improvement. Pullout experiments were performed and analyzed to calculate the work of adhesion for different modifications of the Ti6Al4V surface. PDA layers were applied on Ti6Al4V wire surfaces, followed by a poly(methyl methacrylate-*co*-methacrylic acid) (P(MMA-*co*-MAA)) copolymer coating step on the PDA. The copolymer was applied to ensure the compatibility of PDA with the PMMA matrix, i.e., the copolymer should be capable of reacting with the PDA layer and is expected to promote the formation of secondary bonds and molecular interdigitation with PMMA. The sample design for pullout experiments and the schemes of the surface-modified structures are shown in Figure 2. The overall adhesion of the joint was optimized by tuning the MMA-to-methacrylic acid (MAA) ratio of the copolymer.

2. EXPERIMENTAL SECTION

2.1. Materials. Azobisisobutyronitrile (AIBN; molar mass (M): 164.21 g mol^{-1}), 4-cyano-4-(thiobenzoylthio)pentanoic acid (M: 279.38 g mol^{-1}), methacrylic acid (MAA; M: 86.09 g mol^{-1}), methyl methacrylate (MMA; M: 100.12 g mol^{-1}), aluminum oxide (Al_2O_3), dopamine hydrochloride (M: 189.64 g mol^{-1}), tris(hydroxymethyl)-aminomethane buffer (M: 121.14 g mol^{-1}), potassium hydroxide (KOH), and deuterated dimethyl sulfoxide (DMSO)-d_6 were purchased from Sigma-Aldrich (Zwijndrecht, the Netherlands). Titanium grade 5 wires (Ti6Al4V) with a 1 mm diameter and an average RMS surface roughness value of 2 μm were purchased from SELFAN Fine + Metal GmbH (Köln, Germany). Altuglas PMMA granules were acquired from Resinex (Deventer, the Netherlands). Toluene, acetone, 2-propanol, and *N*,*N*-dimethylformamide (DMF) were obtained from VWR (Amsterdam, the Netherlands). All chemicals were used as received, with the exception of AIBN, which was crystallized from methanol prior to use.

2.2. P(MMA-*co*-MAA) Synthesis. A typical P(MMA-*co*-MAA) reversible addition fragmentation chain transfer (RAFT)[44] polymerization was as follows: Initially, MMA and MAA were passed through a neutral Al_2O_3 column to remove the inhibitor. To 20 mL of anhydrous DMF in a 50 mL Erlenmeyer flask, 7.1×10^{-2} mol of MMA and MAA monomers (ratios specified below), 3.6×10^{-5} mol of RAFT agent, and 2.7×10^{-5} mol of AIBN were added, and the solution was degassed for 30 min using a nitrogen stream. Subsequently, a sample was taken for nuclear magnetic resonance (NMR) analysis and the solution was degassed for 10 more min. Next, the flask was immersed in a silicon oil bath at 70 °C and the solution was allowed to react for 24 h, after which another NMR sample was taken. In total, seven different compositions of P(MMA-*co*-MAA) were synthesized using the following MMA-to-MAA molar ratios: 100:0, 90:10, 80:20, 70:30, 60:40, 50:50, and 0:100.

2.3. Wire Cleaning. The Ti6Al4V wire was straightened with a force of 730 N for 5 min using a tensile testing instrument (Zwick i-line Z5.0, Zwick/Roel, Ulm, Germany) and then cut into 9 cm long pieces. One tip (the embedded tip) of the pieces was polished using 320-grit sandpaper and then 800-grit sandpaper. Subsequently, the wires were ultrasonically cleaned (2510 ultrasonic cleaner; Branson, Danbury) in different solvents, first in toluene and then in acetone, Milli-Q water (Milli-Q Advantage A10, Millipore), and isopropanol, with each cleaning lasting 30 min. Then, the wires were dried at 200 °C under vacuum overnight and stored in a sealed cylindrical container. These wires are hereafter referred to as "clean wires".

2.4. PDA Wire Coating.[21] To modify the Ti6Al4V wires with PDA, clean wires were treated with oxygen plasma (Plasma Prep II SPI; West

https://doi.org/10.1021/acsami.1c01070
ACS Appl. Mater. Interfaces 2021, 13, 19244−19253

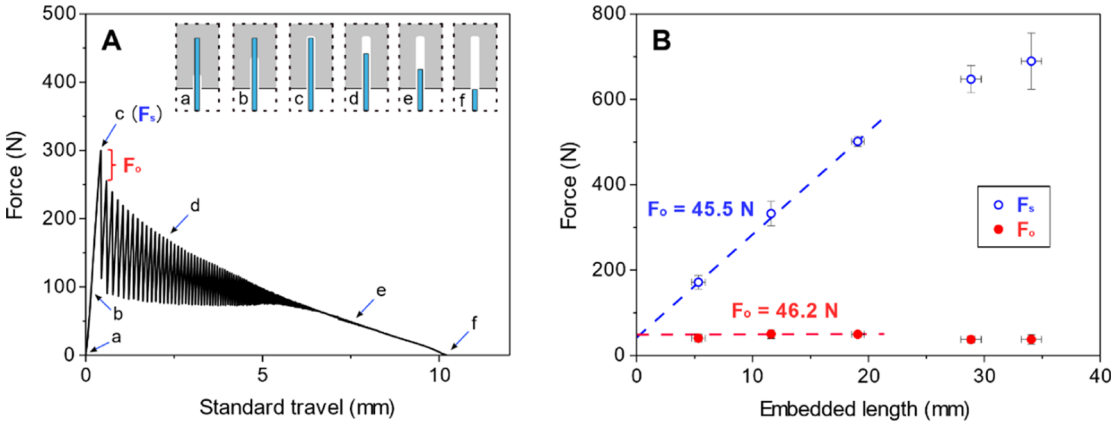

Figure 4. Example wire pullout curve depicting F_s and F_o (A) and F_s and F_o versus embedded length (B) of a PMMA-titanium joint using unmodified Ti wires.

Chester) for 1 min using a current of 40 mA at an oxygen pressure of 200 mTorr. Following plasma treatment, the wires were immediately immersed in a freshly prepared tris buffer solution (10 mM, pH = 9 [KOH]) containing dopamine hydrochloride (5 mg mL^{-1}) and allowed to stand for 24 h under ambient conditions. Finally, the wires were removed from the solution, cleaned thoroughly with Milli-Q water, and dried overnight under vacuum at room temperature. The PDA-coated wires were then stored in a container for 24 h before being used for their respective experiments.

2.5. P(MMA-*co*-MAA) Wire Coating. To coat the Ti6Al4V wires with P(MMA-*co*-MAA), clean or PDA-coated wires were taped onto a 20 × 20 × 1.0 mm^3 titanium platelet, and the polished tip was immersed 2 cm deep in a P(MMA-*co*-MAA)/DMF solution (200 mg mL^{-1}). The sample then underwent spin drying (using a P6700 Specialty Coating Systems) at 1000 rpm for 1 min. Finally, the P(MMA-*co*-MAA)-coated wires were dried under vacuum at room temperature or 150 °C overnight and stored in a cylindrical container.

2.6. PMMA-Ti6Al4V Wire Comolding Process. Specimens for the pullout tests were prepared by compression molding using a mold designed for this process (see Figure 3). Compartments (40 × 20 × 4 mm^3) of the mold were isolated with glass fiber-reinforced Teflon strips. Modified Ti6Al4V wires were guided through these strips, and the mold compartments were filled with PMMA granules. The construct was then pressed (THB 400; Fontijne, Delft, the Netherlands) between two glass fiber-reinforced Teflon sheets with a pressure of 40 MPa at 200 °C for 10 min and cooled to room temperature (30 min cooling time). The samples were demolded and stored under ambient conditions for 24 h before being subjected to the pullout tests. A schematic of the overall process is shown in Figure 3.

2.7. Pullout Process. The comolded samples were subjected to pullout tests (Zwick i-line Z5.0, Zwick/Roel, Ulm, Germany) using two modified grips (see Supporting Information SI 1) at a crosshead speed of 10 mm min^{-1}. At least five specimens were tested for each sample configuration.

2.8. Characterization Methods. Nuclear magnetic resonance (^{1}H NMR) (Avance III (400 MHz); Bruker) was used to determine the degree of polymerization and conversion and the MMA-to-MAA ratio of the copolymers using DMSO-d_6 as the solvent. Example NMR spectra are shown and discussed in Supporting Information SI 2. Fourier transform infrared (FTIR) spectroscopy (Alpha, Bruker) and thermogravimetric analysis (TGA; TGA550, TA Instruments) of the copolymers were also performed. In a typical process, 0.3 mL of a P(MMA-*co*-MAA) solution in DMF (200 mg mL^{-1})—similar to that used during spin drying (see Section 2.5)—was poured on a Teflon sheet, followed by drying and annealing under vacuum overnight at 150 °C. The resulting samples were separated from the Teflon sheets and subjected to thermogravimetric analysis (TGA) and Fourier transformed infrared (FTIR) spectroscopy measurements. TGA was performed in a N_2 atmosphere from 50 to 500 °C at a rate of 20 °C min^{-1}. FTIR (ATR mode) was performed from 4000 to 400 cm^{-1}, and 64 scans were performed at a resolution of 4 cm^{-1}. The FTIR spectra were subjected to baseline correction and smoothening (25 points). The TGA and FTIR data, as well as their analysis, are shown in Supporting Information SI 3.

X-ray photoelectron spectroscopy (XPS; Quantera SXM, Physical Electronics) was performed on the clean and PDA-coated Ti6Al4V wire surfaces to verify the successful formation of the PDA layer. A monochromatic Al Kα radiation source at 1486.6 eV was used with a 100 μm diameter beam and 25 W X-ray gun power. The base pressure of the chamber was 5.4 × 10^{-10} Torr, and the working pressure was 3.0 × 10^{-8} Torr (argon). The beam input and detector input angles were 45°. The obtained XPS spectra along with their respective analysis are shown in Supporting Information SI 4.

Scanning electron microscopy (SEM) (JSM 7610 FPlus; JEOL) was used to image the surface morphology of the Ti6Al4V wires, measure the thickness of the copolymer coatings and evaluate the type of interfacial failure of the wires following pullout testing. Prior to the cross-sectional SEM analysis, the modified wires before and after the pullout tests were immersed in liquid N_2 for 2 min before being cut. The acceleration voltage was 1.5 kV, and the working distance (W.D.) was 11.4 mm. Energy-dispersive X-ray spectroscopy (EDX) was performed to provide further information on the interfacial failure mode using an EDX detector (Oxford Instruments AztecLive Standard Ultim 40 mm^2, 127 eV) equipped on an electron microscope. The obtained EDX spectra along with their analysis are shown in Supporting Information SI 5.

3. RESULTS AND DISCUSSION

3.1. Testing Method and Analysis. First, we display and discuss the results of the pullout tests for the unmodified Ti wires. Figure 4A shows a typical force-crosshead standard travel pullout curve of a clean Ti wire−PMMA comolded joint. Initially, a linear increase in the force with standard travel was observed. In this region, the existing crack formed during cooling (see Figure 3) propagated toward the embedded end (see the schematic in Figure 4A). The complete propagation of the crack occurred at the slip point, where the wire moved with respect to the matrix for the first time. Past the slip point, the wire was progressively removed from the embedded matrix, initially in a stick-and-slip manner, followed by frictional sliding, until the wire was completely separated from the embedded matrix. "Stick-and-slip oscillations" (section d in Figure 4A) have been previously observed in pullout experiments and were assigned to the difference between the static and dynamic friction coefficients, as well as to the Poisson contraction of fibers.[40,45] The amplitude of the oscillations depended on the force to initiate the slip of the wire[46] and was gradually reduced

https://doi.org/10.1021/acsami.1c01070
ACS Appl. Mater. Interfaces 2021, 13, 19244−19253

with the removal of the wire from the matrix to result in frictional sliding (section e in Figure 4A).

To interpret the results obtained by the pullout experiments, the theory originally introduced by Outwater and Murphy[47] was employed. This particular analysis describes the debonding of a ductile fiber from a brittle matrix using Griffith's fracture criterion.[41] Bowling and Groves,[48] based on the theory of Outwater and Murphy, expressed the force at the slip point (F_s) (indicated as c in Figure 4A) as

$$F_s = 2\pi r^{3/2}(E_f G_a)^{1/2} + 2\pi r L \tau_f \quad (1)$$

where r is the diameter of the fiber, E_f is the modulus of the fiber, G_a is the work of adhesion, L is the embedded length, and τ_f is the interfacial stress between the embedded fiber and polymer matrix following debonding. Equation 1 contains two terms, namely, the adhesion term that corresponds to the force required to detach the interface (or initiate crack propagation) and the frictional term that corresponds to the frictional interaction at the detached fiber-matrix interface. To estimate G_a, the frictional term of eq 1 needs to be excluded, which results in

$$F_o = 2\pi r^{3/2}(E_f G_a)^{1/2} \quad (2)$$

where F_o is the force required to initiate crack propagation.

According to the analysis of Wang,[41] there were two potential methods to exclude the interfacial stress term in eq 1 and determine the value of F_o.[41] The first approach included subtracting the force at the first stick-and-slip point (see Figure 4A) from the slip force. The second method involved plotting the values of F_s versus L and extrapolating the curve to an embedded length of zero. As a result, we obtained the force required to pull out the fiber under no-friction conditions (see eq 1).[48,49] Figure 4B shows the dependence of F_s and F_o on the embedded length (L). It can clearly be seen that the value of F_o was independent of L. In addition, the value of F_s showed a linear dependence on L at low L values, whereas a deviation from linearity was observed at higher L values. The dependence of both F_s and F_o on L had been experimentally observed and reported by Wang in a poly(tetrafluoroethylene) (PTFE) fiber-polypropylene system.[41] Our observations can be explained by the Bowling and Groves analysis[48] (eq 1) for low–medium L values (eq 1). The deviation from linearity observed for higher L values was tentatively attributed to the Poisson contraction of wire at higher force values.[50] Using L values below 2 cm, the value of F_o was determined with the methods discussed above and was found to be 46.2 ± 5.5 and 45.5 ± 8.1 N, respectively; see Figure 4B. The good agreement of the F_o values calculated using the two different methods, in combination with the observed dependence of F_o and F_s on L, verified the applicability of Wang's analysis on the PMMA-Ti system presented in this study.

Using 46.2 N as a value for F_o, a diameter of 1 mm, and a wire modulus of 114 GPa in eq 2, a value of 3.8 J m^{-2} was obtained for the work of adhesion (G_a) between Ti and PMMA. To the extent of our knowledge, no values have been reported in the literature for the interfacial adhesive energy (i.e., energy per unit area) between Ti and PMMA; instead, interfacial adhesion has been discussed in terms of tensile or shear stress.[51−57] These values are highly dependent on the morphology of the Ti surface as well as on the testing method, which makes a comparison with the results presented in this study speculative. However, Aminabhavi and co-workers[58] reported the use of molecular dynamics simulations to calculate the interaction energy between an MMA monomer and different titanium oxide surfaces, which ranged from 1.78 to 2.08 J m^{-2}. Our experimentally determined value of G_a was on the same order of magnitude. Exceeding the simulated value could be a result of several factors, including the assumptions made in the simulations,[58] as well as in Wang's model,[41] such as the assumed inextensibility of the polymer matrix, the actual surface composition of Ti, and the effect of surface roughness.

3.2. Pullout Tests on Surface-Modified Wires. As previously mentioned, to promote adhesion in the PMMA-Ti joint, a two-step surface modification of Ti was performed. In the first step, a PDA layer with a thickness of a few tens of nm was formed, to which in the second step, a P(MMA-*co*-MAA) thin film was added. The complete surface coverage of Ti by PDA was verified by XPS (see Supporting Information SI 4). Successful copolymer synthesis was verified by NMR. The NMR data were used to obtain the values of Mn and the MMA/MAA composition of the copolymers (see Supporting Information SI 2).

Figure 5 shows the values of F_o versus the MAA content of the copolymer layer. The F_o values clearly increased with the MAA

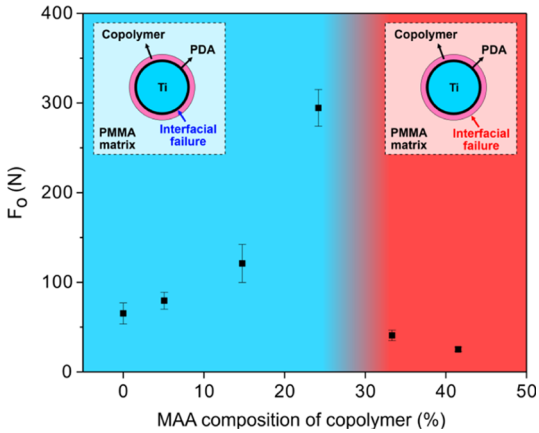

Figure 5. F_o versus the MAA content of the copolymer layer on the PDA-modified Ti wire. The blue region represents failure at the copolymer−Ti interface, and the red region corresponds to failure at the copolymer−matrix interface, as represented by the schematic cross sections in the insets.

content until approximately 24% (light blue region; Figure 5). Regarding higher MAA contents, F_o showed a sharp drop followed by a decreasing trend as the MAA content increased (red region; Figure 5). This behavior was unexpected because it was initially assumed that an increase in MAA content would continuously increase the interfacial strength due to reaction and covalent bond formation between carboxylic acid and PDA. To obtain further insights into the origins of this unexpected behavior, the mode of failure was examined in detail.

SEM was used to image the Ti wire surface. Figure 6A shows the SEM image of a clean wire. After being coated with PDA and copolymer, the interfacial structure is captured at a higher magnification in Figure 6B, clearly depicting the coating layer. Additional images provided information about the interfacial failure modes. Figure 6C,D shows representative images of the wires coated with a copolymer and with MAA content in the blue and red regions of Figure 5, respectively, following pullout testing. The structural differences of the failed interfaces are apparent. Figure 6E,F shows the cross-sectional images of the

https://doi.org/10.1021/acsami.1c01070
ACS Appl. Mater. Interfaces 2021, 13, 19244−19253

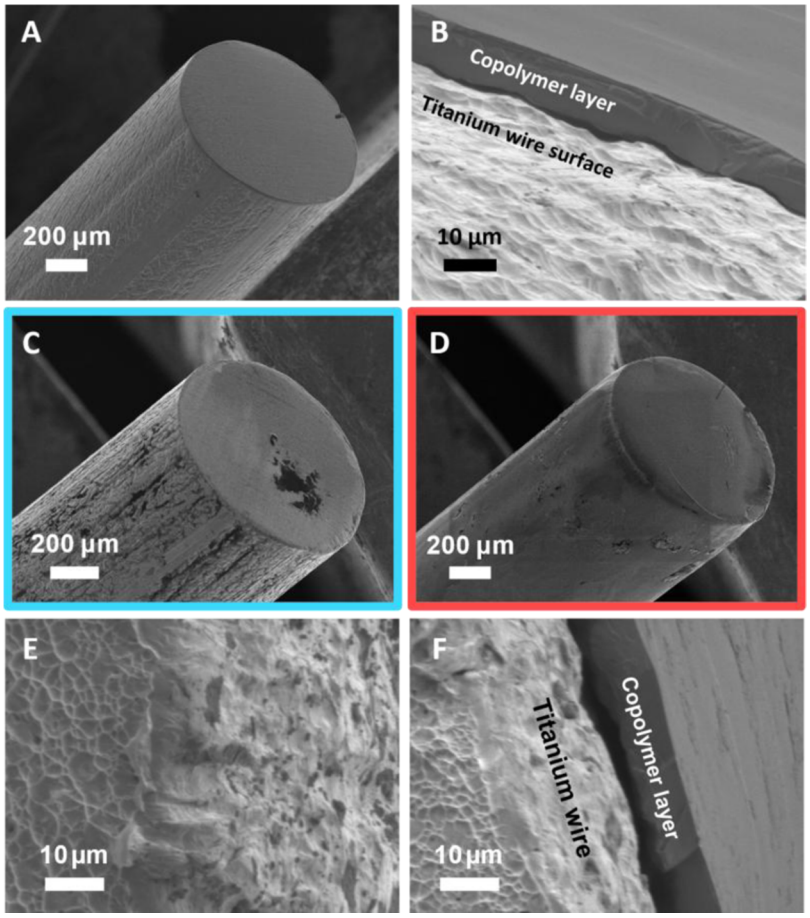

Figure 6. SEM images of (A) a clean Ti wire prior to the comolding process; (B) the cross section of a cut copolymer-coated wire prior to the comolding process; (C) a PDA-copolymer-coated wire with an MAA copolymer content of 15% (blue domain in Figure 5) after pullout testing, showing interfacial failure at the copolymer−Ti interface; (D) a copolymer-coated wire with MAA copolymer content of 42% (red domain in Figure 5) after pullout testing, showing failure at the copolymer−matrix interface; (E) the cryo-fractured wire shown in (C); and (F) the cryo-fractured wire shown in (D).

interfaces for the wires displayed in Figure 6C,D, respectively. Figure 6F reveals that the copolymer layer deposited on the PDA-coated wire remains on the wire surface following pullout. This result is evidence for failure at the copolymer−matrix interface. However, in Figure 6E, the copolymer layer could not be seen anymore. This observation indicated a change in the location of the failed interface, which shifted to occurring between the copolymer layer and Ti surface. In addition to morphology imaging by SEM, we also performed an EDX analysis to monitor the chemical composition of the wire surface following pullout. As we show in the Supporting Information (SI 5), EDX provided further evidence for the conclusions reached above.

Following debonding of the interface during the pullout test, the Ti wire was sheared against the PMMA matrix until the two were completely separated. During this process, "frictional material transfer" was likely to occur between the metal and polymer due to large differences in their respective shear strength values. Regarding Ti−copolymer interfacial failure, this would correspond to material transfer from the polymer to the Ti surface. An example of this can be seen in Figure 6C,E, where the remaining polymer is observed on the Ti surface following pullout. However, this result does not allow us to conclude whether the PDA film indeed remained at the Ti surface; thus, unambiguous identification of the failure location in this case was not feasible. Therefore, for simplicity, we will refer to the Ti−PDA−copolymer system as the copolymer−Ti interface.

Considering all of the above observations, we identify two potential sites of interfacial failure that include the copolymer−Ti (Figure 6C) and copolymer-PMMA matrix (Figure 6D) interfaces. The Ti−copolymer interfacial failure shown in Figure 6C is representative of MAA copolymer compositions up to 24%. Similarly, for MAA compositions of 33% or higher, Figure 6D serves as a representative interfacial failure location.

We interpret these results tentatively by analyzing the functionality of the MAA component of the copolymer coating. Methacrylic acid could react with PDA, forming amide bonds,[24] at the Ti−copolymer interface. The formation of covalent bonds explained the initial trend of increasing F_o with an increasing MAA content of the copolymer. However, MAA also engaged in thermally triggered cross-linking reactions, which were confirmed by TGA and FTIR measurements (see Supporting Information SI 3). This result implied that a higher MAA content in the copolymer yielded a higher degree of cross-linking. Different interactions exist between the PMMA and the copolymer layer. During the comolding process, the fully mobile PMMA matrix was brought into contact with the copolymer coating, enhancing interactions such as secondary forces and molecular interdigitation. The formation of such enhanced interactions was expected to be hindered by the increased degree

https://doi.org/10.1021/acsami.1c01070
ACS Appl. Mater. Interfaces 2021, 13, 19244−19253

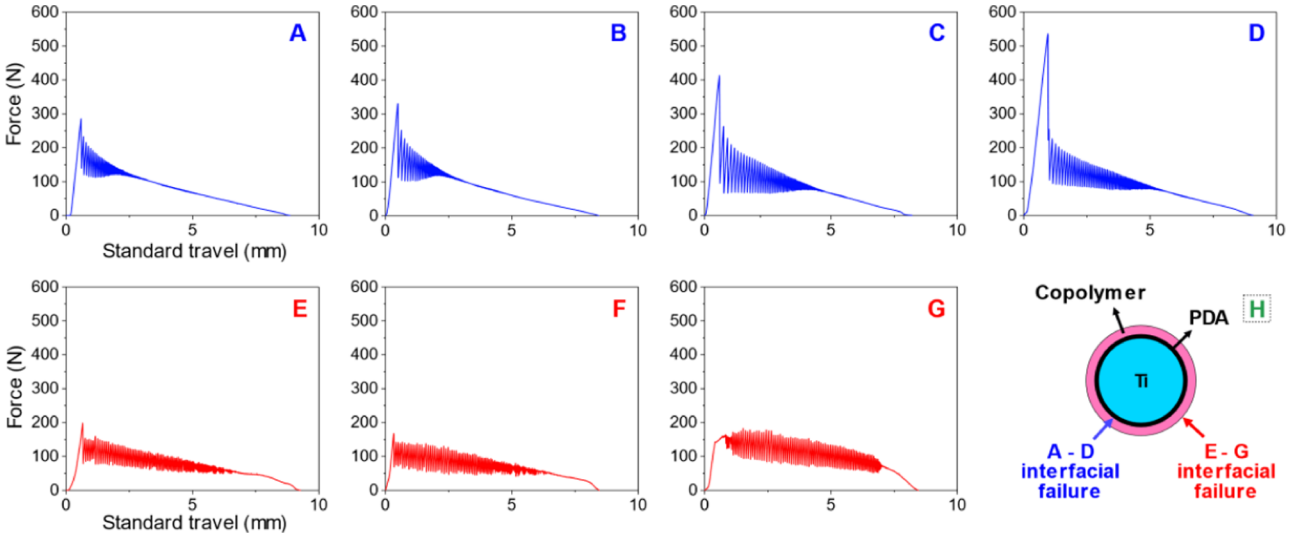

Figure 7. Representative pullout curves of samples prepared by copolymer−PDA-modified wires with copolymers and with MAA contents of 0, 5, 15, 24, 33, 42, and 100% (A−G). Cross-sectional schematic representation of the modified pullout samples (H).

of cross-linking with an increasing MAA concentration. The latter mechanism reduced the strength of the copolymer−PMMA matrix interface. These opposing trends resulted in a maximum in the observed F_o values.

The MAA content at which one interface became stronger than the other was the point at which the maximum adhesion of the joint was observed and the point at which the site of failure changed. This point was expected to be within the transition region at approximately 30% MAA, as seen in Figure 5. The maximum measured F_o was at 24% MAA and was found to be 294.5 N, 6 times the value of unmodified wires. According to eq 2, the interfacial adhesion energy (G_a) at 24% MAA was 155 J m^{-2}. When this value was compared to the fracture toughness of PMMA, i.e., 700−1600 J m^{-2},[59] we could argue that the maximum achieved work of adhesion was approximately 10−20% of the fracture energy of PMMA. It should be noted that the surface of the Ti wires used in this study, as indicated by XPS measurements (see SI 4), contained minor contaminants originating either from atmospheric carbon or processing during wire production. We estimate that this could cause a slight decrease in the maximum bonding strength between PDA and Ti, since the dopamine molecules during PDA film formation would have a reduced TiO_2 area to coordinate to. Nonetheless, the fact that we still observe high bond strength even when not using ideal surfaces further supports the use of the present method for improved interfaces also in technological applications.

Figure 7 presents representative pullout curves for all data points shown in Figure 5, in addition to a wire coated with PDA and PMAA (100% MAA). Remarkably, the stick-and-slip behavior changed significantly when the site of interfacial failure changed from the copolymer−Ti interface (Figure 7A−D, blue region) to the copolymer−matrix interface (Figure 7E,F, red region). The initial "spike" in F_o strongly decreased and eventually disappeared, while the "envelope" of the stick-slip section altered significantly. We attribute these differences to the changes in the interfacial properties from one interface to the other. We note that the change in the frictional profile (the stick-slip envelope) could provide a rapid method to identify the site of interfacial failure. The plots of the samples that showed failure at the copolymer−Ti interface (Figure 7A−D) suggested that although the slip force increased with the MAA content, the first stick-and-slip point remained constant at approximately 250 N. This result was in good agreement with the predictions of eq 1, providing further proof that the particular analysis employed here could describe the results of the testing method used in the present study.

To verify the interaction between PDA and the copolymer layers for the copolymer with 24% MAA, which showed the highest interfacial strength, a control experiment was performed. A comparison of the F_o values obtained for an unmodified, PDA-coated, copolymer-coated, and PDA−copolymer-coated wire is shown in Figure 8. With respect to the unmodified Ti wire, the

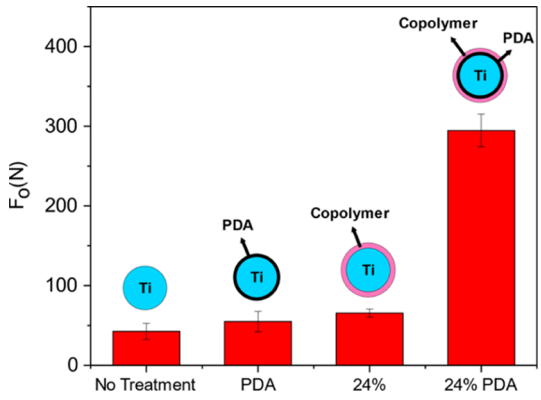

Figure 8. F_o values of the different surface modifications of Ti wires. In this case, 24% represents the P(MMA-*co*-MAA) copolymer with 24% MAA content.

application of a PDA layer did not show any significant increase in the F_o values. This result indicated that the PMMA matrix could not efficiently participate in a thermally triggered reaction with PDA; thus, no enhanced adhesion was observed. Similar results were observed with the copolymer coating, with only a slight increase in the F_o values. Regarding the wire with the combined coating, a dramatic increase in the F_o value was observed in comparison to the other cases. This increase clearly showed that the interaction between the subsequently deposited

https://doi.org/10.1021/acsami.1c01070
ACS Appl. Mater. Interfaces 2021, 13, 19244−19253

layers resulted in a significantly strengthened interface of the combined coating.

4. CONCLUSIONS

We demonstrated the effect of a PDA−copolymer double-layer surface modification of a metal to significantly improve the adhesion of a TPM−metal comolded joint. Comolded joints of PMMA and (modified) titanium grade 5 (Ti6Al4V) wires were prepared by compression molding and subjected to pullout tests. The pullout testing method was analyzed using the modified theory of Outwater and Murphy[47] introduced by Bowling and Groves.[48] Our results were in excellent agreement with the theoretical predictions. The application of PDA on the Ti surface did not show any significant improvements in adhesion. This result indicated that PMMA and PDA did not engage in a thermally triggered reaction. Adhesion was engineered by the application of a P(MMA-*co*-MAA) coating on PDA-modified Ti. By increasing the MAA content of the copolymer, a failure transition from the copolymer−Ti to the copolymer−PMMA interface was observed. We interpreted this change as follows: an increase in the MAA content strengthened the copolymer−Ti interface by the formation of more amide bonds between MAA and PDA. However, the thermal cross-linking of the MAA moieties weakened the copolymer−PMMA interface by preventing the formation of secondary bonds and molecular interdigitation. This mechanism explained the change in the interfacial failure location as well as the observed maximum F_o values for the different copolymer compositions. A copolymer with 24% MAA showed the maximum interfacial strength, that is, 6 times the strength of unmodified Ti, which could not be further improved due to the cross-linking of the MAA moieties. The P(MMA-*co*-MAA) coating did not perform as well in the absence of PDA, indicating the synergistic interaction between the layers. Overall, PDA was demonstrated to be thermally stable in terms of adhesion, with high potential for future TPM−metal comolding applications.

■ ASSOCIATED CONTENT

Supporting Information

The Supporting Information is available free of charge at https://pubs.acs.org/doi/10.1021/acsami.1c01070.

> Wire pullout setup; P(MMA-*co*-MAA) copolymer NMR; TGA and FTIR of P(MMA-*co*-MAA) annealed copolymers; XPS spectra of unmodified and PDA modified Ti_6Al_4V wires; and EDX surface analysis (PDF)

■ AUTHOR INFORMATION

Corresponding Authors

Joost Duvigneau − *Department of Materials Science and Technology of Polymers, University of Twente, Enschede 7522 NB, the Netherlands;* orcid.org/0000-0002-2810-2768; Email: j.duvigneau@utwente.nl

G. Julius Vancso − *Department of Materials Science and Technology of Polymers, University of Twente, Enschede 7522 NB, the Netherlands;* orcid.org/0000-0003-4718-0507; Email: g.j.vancso@utwente.nl

Authors

Georgios Kafkopoulos − *Department of Materials Science and Technology of Polymers, University of Twente, Enschede 7522 NB, the Netherlands*

Clemens J. Padberg − *Department of Materials Science and Technology of Polymers, University of Twente, Enschede 7522 NB, the Netherlands*

Complete contact information is available at: https://pubs.acs.org/10.1021/acsami.1c01070

Notes

The authors declare no competing financial interest.

■ ACKNOWLEDGMENTS

This work was performed as part of the HTSM2017 research program under project number 16213, which is (partly) financed by the Dutch Research Council (NWO). The authors also gratefully acknowledge the support from the ThermoPlastic Composites Research Center (TPRC). The authors also acknowledge Dr. Ir. W. Grouve for his advice on the pullout analysis.

■ REFERENCES

(1) Grujicic, M.; Sellappan, V.; Kotrika, S.; Arakere, G.; Obieglo, A.; Erdmann, M.; Holzleitner, J. Suitability Analysis of a Polymer-Metal Hybrid Technology Based on High-Strength Steels and Direct Polymer-to-Metal Adhesion for Use in Load-Bearing Automotive Body-in-White Applications. *J. Mater. Process. Technol.* **2009**, *209*, 1877−1890.

(2) Grujicic, M.; Sellappan, V.; Omar, M. A.; Seyr, N.; Obieglo, A.; Erdmann, M.; Holzleitner, J. An Overview of the Polymer-to-Metal Direct-Adhesion Hybrid Technologies for Load-Bearing Automotive Components. *J. Mater. Process. Technol.* **2008**, *197*, 363−373.

(3) Drummer, D.; Schmachtenberg, E.; Hülder, G.; Meister, S. MK2 - A Novel Assembly Injection Molding Process for the Combination of Functional Metal Surfaces with Polymer Structures. *J. Mater. Process. Technol.* **2010**, *210*, 1852−1857.

(4) Yin, S.; Xie, Y.; Li, R.; Zhang, J.; Zhou, T. Polymer-Metal Hybrid Material with an Ultra-High Interface Strength Based on Mechanical Interlocking via Nanopores Produced by Electrochemistry. *Ind. Eng. Chem. Res.* **2020**, *59*, 12409−12420.

(5) Lambiase, F. Mechanical Behaviour of Polymer-Metal Hybrid Joints Produced by Clinching Using Different Tools. *Mater. Des.* **2015**, *87*, 606−618.

(6) Shishesaz, M.; Hosseini, M. Effects of Joint Geometry and Material on Stress Distribution, Strength and Failure of Bonded Composite Joints: An Overview. *J. Adhes.* **2020**, *96*, 1053−1121.

(7) Kleffel, T.; Drummer, D. Investigating the Suitability of Roughness Parameters to Assess the Bond Strength of Polymer-Metal Hybrid Structures with Mechanical Adhesion. *Composites, Part B* **2017**, *117*, 20−25.

(8) Lee, L.-H. Molecular Bonding and Adhesion at Polymer-Metal Interphases. *J. Adhes.* **1994**, *46*, 15−38.

(9) Mallakpour, S.; Madani, M. A Review of Current Coupling Agents for Modification of Metal Oxide Nanoparticles. *Prog. Org. Coat.* **2015**, *86*, 194−207.

(10) Schulze, K.; Hausmann, J.; Wielage, B. The Stability of Different Titanium-PEEK Interfaces against Water. *Procedia Mater. Sci.* **2013**, *2*, 92−102.

(11) Molitor, P.; Barron, V.; Young, T. Surface Treatment of Titanium for Adhesive Bonding to Polymer Composites: A Review. *Int. J. Adhes. Adhes.* **2001**, *21*, 129−136.

(12) Critchlow, G. W.; Brewis, D. M. Review of Surface Pretreatments for Titanium Alloys. *Int. J. Adhes. Adhes.* **1995**, *15*, 161−172.

(13) Liu, Y.; Ai, K.; Lu, L. Polydopamine and Its Derivative Materials: Synthesis and Promising Applications in Energy, Environmental, and Biomedical Fields. *Chem. Rev.* **2014**, *114*, 5057−5115.

(14) Barclay, T. G.; Hegab, H. M.; Clarke, S. R.; Ginic-Markovic, M. Versatile Surface Modification Using Polydopamine and Related Polycatecholamines: Chemistry, Structure, and Applications. *Adv. Mater. Interfaces* **2017**, *4*, No. 1601192.

(15) Chakraborty, A. K.; Davis, H. T.; Tirrell, M. A Molecular Orbital Study of the Interactions of Acrylic Polymers with Aluminum: Implications for Adhesion. *J. Polym. Sci., Part A: Polym. Chem.* **1990**, *28*, 3185−3219.
(16) Merkel, D. R.; Laursen, C. M.; Yakacki, C. M.; Rorrer, R. A.; Frick, C. P. Characterization and Mechanical Testing of Polydopamine-Adhered Electroless Copper Films. *Surf. Coatings Technol.* **2017**, *331*, 211−220.
(17) Klosterman, L.; Ahmad, Z.; Viswanathan, V.; Bettinger, C. J. Synthesis and Measurement of Cohesive Mechanics in Polydopamine Nanomembranes. *Adv. Mater. Interfaces* **2017**, *4*, No. 1700041.
(18) Li, Y.; Cao, Y. The Molecular Mechanisms Underlying Mussel Adhesion. *Nanoscale Adv.* **2019**, *1*, 4246−4257.
(19) Zhang, C.; Gong, L.; Xiang, L.; Du, Y.; Hu, W.; Zeng, H.; Xu, Z. K. Deposition and Adhesion of Polydopamine on the Surfaces of Varying Wettability. *ACS Appl. Mater. Interfaces* **2017**, *9*, 30943−30950.
(20) Li, W.; Li, Y.; Sheng, M.; Cui, S.; Wang, Z.; Zhang, X.; Yang, C.; Yu, Z.; Zhang, Y.; Tian, S.; Dai, Z.; Xu, Q. Enhanced Adhesion of Carbon Nanotubes by Dopamine Modification. *Langmuir* **2019**, *35*, 4527−4533.
(21) Lee, H.; Dellatore, S.; Miller, W.; Messersmith, P. Mussel-Inspired Surface Chemistry for Multifunctional Coatings. *Science* **2007**, *318*, 426−430.
(22) Bahri, S.; Jonsson, C. M.; Jonsson, C. L.; Azzolini, D.; Sverjensky, D. A.; Hazen, R. M. Adsorption and Surface Complexation Study of L-DOPA on Rutile (α-TiO2) in NaCl Solutions. *Environ. Sci. Technol.* **2011**, *45*, 3959−3966.
(23) Jackman, M. J.; Syres, K. L.; Cant, D. J. H.; Hardman, S. J. O.; Thomas, A. G. Adsorption of Dopamine on Rutile TiO2 (110): A Photoemission and near-Edge x-Ray Absorption Fine Structure Study. *Langmuir* **2014**, *30*, 8761−8769.
(24) Wang, L.; Wang, D.; Dong, Z.; Zhang, F.; Jin, J. Interface Chemistry Engineering for Stable Cycling of Reduced GO/SnO_2 Nanocomposites for Lithium Ion Battery. *Nano Lett.* **2013**, *13*, 1711−1716.
(25) Wang, L.; Dong, Z.; Wang, D.; Zhang, F.; Jin, J. Covalent Bond Glued Sulfur Nanosheet-Based Cathode Integration for Long-Cycle-Life Li-S Batteries. *Nano Lett.* **2013**, *13*, 6244−6250.
(26) Malollari, K. G.; Delparastan, P.; Sobek, C.; Vachhani, S. J.; Fink, T. D.; Zha, R. H.; Messersmith, P. B. Mechanical Enhancement of Bioinspired Polydopamine Nanocoatings. *ACS Appl. Mater. Interfaces* **2019**, *11*, 43599−43607.
(27) Saiz-Poseu, J.; Mancebo-Aracil, J.; Nador, F.; Busqué, F.; Ruiz-Molina, D. The Chemistry behind Catechol-Based Adhesion. *Angew. Chem., Int. Ed.* **2019**, *58*, 696−714.
(28) Li, Y.-h.; Zhou, M.; Geng, C.-z.; Chen, F.; Fu, Q. Simultaneous Improvements of Thermal Stability and Mechanical Properties of Poly(Propylene Carbonate) via Incorporation of Environmental-Friendly Polydopamine. Chinese. *J. Polym. Sci.* **2014**, *32*, 1724−1736.
(29) Liu, Y.; Fang, Y.; Qian, J.; Liu, Z.; Yang, B.; Wang, X. Bio-Inspired Polydopamine Functionalization of Carbon Fiber for Improving the Interfacial Adhesion of Polypropylene Composites. *RSC Adv.* **2015**, *5*, 107652−107661.
(30) Zhang, L.; Li, Z.; Pan, Y. T.; Yáñez, A. P.; Hu, S.; Zhang, X. Q.; Wang, R.; Wang, D. Y. Polydopamine Induced Natural Fiber Surface Functionalization: A Way towards Flame Retardancy of Flax/Poly(Lactic Acid) Biocomposites. *Composites, Part B* **2018**, *154*, 56−63.
(31) Zheng, Y.; Wang, X.; Wu, G. Facile Strategy of Improving Interfacial Strength of Silicone Resin Composites through Self-Polymerized Polydopamine Followed via the Sol-Gel Growing of Silica Nanoparticles onto Carbon Fiber. *Polymers* **2019**, *11*, 1639.
(32) Wang, H.; Cao, J.; Luo, F.; Cao, C.; Qian, Q.; Huang, B.; Xiao, L.; Chen, Q. Simultaneously Enhanced Mechanical Properties and Flame Retardancy of UHMWPE with Polydopamine-Coated Expandable Graphite. *RSC Adv.* **2019**, *9*, 21371−21380.
(33) Georgopanos, P.; Eichner, E.; Filiz, V.; Handge, U. A.; Schneider, G. A.; Heinrich, S.; Abetz, V. Improvement of Mechanical Properties by a Polydopamine Interface in Highly Filled Hierarchical Composites of Titanium Dioxide Particles and Poly(Vinyl Butyral). *Compos. Sci. Technol.* **2017**, *146*, 73−82.
(34) Zhou, S.; Gao, J.; Wang, J.; Wang, S.; Yue, J.; Dong, C.; Huang, J.; Zhao, G.; Liu, Y. Polydopamine-Coupling of Carbon Nanotubes onto Microscaled Basalt Fiber to Enhancing Mechanical, Thermal and Tribological Properties of Composite Materials. *Mater. Res. Express* **2019**, *6*, No. 0850g6.
(35) Martin, A.; Addiego, F.; Mertz, F.; BArdon, J.; Ruch, D.; Dubois, P. Pitch-Based Carbon Fibre-Reinforced PEEK Composites: Optimization of Interphase Properties by Water-Based Treatments and Self-Assembly. *J. Mater. Sci. Eng.* **2016**, *6*, No. 1000308.
(36) Phua, S. L.; Yang, L.; Toh, C. L.; Guoqiang, D.; Lau, S. K.; Dasari, A.; Lu, X. Simultaneous Enhancements of UV Resistance and Mechanical Properties of Polypropylene by Incorporation of Dopamine-Modified Clay. *ACS Appl. Mater. Interfaces* **2013**, *5*, 1302−1309.
(37) Chug, P. S.; Piggott, M. R. Mechanical Properties of the Glass Fibre-Polyester Interphase. *J. Mater. Sci.* **1992**, *27*, 925−929.
(38) Antico, F. C.; Zavattieri, P. D.; Hector, L. G.; Mance, A.; Rodgers, W. R.; Okonski, D. A. Adhesion of Nickeltitanium Shape Memory Alloy Wires to Thermoplastic Materials: Theory and Experiments. *Smart Mater. Struct.* **2012**, *21*, No. 035022.
(39) Piggott, M. R. The Interface in Carbon Fibre Composites. *Carbon* **1989**, *27*, 657−662.
(40) Chua, P. S.; Piggott, M. R. The Glass Fibre-Polymer Interface: II-Work of Fracture and Shear Stresses. *Compos. Sci. Technol.* **1985**, *22*, 107−119.
(41) Wang, C. Fracture Mechanics of Single-Fibre Pull-out Test. *J. Mater. Sci.* **1997**, *32*, 483−490.
(42) Piggott, M. R.; Dai, S. R. Fiber Pull out Experiments with Thermoplastics. *Polym. Eng. Sci.* **1991**, *31*, 1246−1249.
(43) Ozkan, T.; Chen, Q.; Chasiotis, I. Interfacial Strength and Fracture Energy of Individual Carbon Nanofibers in Epoxy Matrix as a Function of Surface Conditions. *Compos. Sci. Technol.* **2012**, *72*, 965−975.
(44) Perrier, S. 50th Anniversary Perspective: RAFT Polymerization - A User Guide. *Macromolecules* **2017**, *50*, 7433−7447.
(45) Chua, P. S.; Piggott, M. R. The Glass Fibre-Polymer Interface: I-Theoretical Consideration for Single Fibre Pull-out Tests. *Compos. Sci. Technol.* **1985**, *22*, 33−42.
(46) Chua, P. S.; Piggott, M. R. The Glass Fibre-Polymer Interface: III-Pressure and Coefficient of Friction. *Compos. Sci. Technol.* **1985**, *22*, 185−196.
(47) Bowling, J.; Groves, G. W. The Debonding and Pull-out of Ductile Wires from a Brittle Matrix. *J. Mater. Sci.* **1979**, *14*, 431−442.
(48) Gray, R. J. Analysis of the Effect of Embedded Fibre Length on Fibre Debonding and Pull-out from an Elastic Matrix - Part 1 Review of Theories. *J. Mater. Sci.* **1984**, *19*, 861−870.
(49) Gent, A. N.; Liu, G. L. Pull-out and Fragmentation in Model Fibre Composites. *J. Mater. Sci.* **1991**, *26*, 2467−2476.
(50) Takaku, A.; Arridge, R. G. C. The Effect of Interfacial Radial and Shear Stress on Fibre Pull-out in Composite Materials. *J. Phys. D. Appl. Phys.* **1973**, *6*, 2038−2047.
(51) Bulbul, M.; Kesim, B. The Effect of Primers on Shear Bond Strength of Acrylic Resins to Different Types of Metals. *J. Prosthet. Dent.* **2010**, *103*, 303−308.
(52) Matinlinna, J. P.; Özcan, M.; Lassila, L. V. J.; Vallittu, P. K. The Effect of a 3-Methacryloxypropyltrimethoxysilane and Vinyltriisopropoxysilane Blend and Tris(3-Trimethoxysilylpropyl)Isocyanurate on the Shear Bond Strength of Composite Resin to Titanium Metal. *Dent. Mater.* **2004**, *20*, 804−813.
(53) Ohkubo, C.; Watanabe, I.; Hosoi, T.; Okabe, T. Shear Bond Strengths of Polymethyl Methacrylate to Cast Titanium and Cobalt-Chromium Frameworks Using Five Metal Primers. *J. Prosthet. Dent.* **2000**, *83*, 50−57.
(54) Stepuk, A.; Halter, J. G.; Schaetz, A.; Grass, R. N.; Stark, W. J. Mussel-Inspired Load Bearing Metal-Polymer Glues. *Chem. Commun.* **2012**, *48*, 6238−6240.

https://doi.org/10.1021/acsami.1c01070
ACS Appl. Mater. Interfaces 2021, 13, 19244−19253

(55) Kim, S.-S.; Vang, M.-S.; Yang, H.-S.; Park, S.-W.; Lim, H.-P. Effect of Adhesive Primers on Bonding Strength of Heat Cure Denture Base Resin to Cast Titanium and Cobalt-Chromium Alloy. *J. Adv. Prosthodont.* **2009**, *1*, 41−46.
(56) May, K. B.; Razzoog, E.; Lang, R.; Arbor, A. Silane to enhance the bond between polymethyl methacrylate and titanium. *J. Adv. Prosthodont.* **1995**, *73*, 428−431.
(57) Hamming, L. M.; Fan, X. W.; Messersmith, P. B.; Brinson, L. C. Mimicking Mussel Adhesion to Improve Interfacial Properties in Composites. *Compos. Sci. Technol.* **2008**, *68*, 2042−2048.
(58) Prathab, B.; Subramanian, V.; Aminabhavi, T. M. Molecular Dynamics Simulations to Investigate Polymer-Polymer and Polymer-Metal Oxide Interactions. *Polymer.* **2007**, *48*, 409−416.
(59) Ku, H. S.; Baddeley, D.; Snook, C.; Chew, C. S. Fracture Toughness of Vinyl Ester Composites Cured by Microwave Irradiation: Preliminary Results. *J. Reinf. Plast. Compos.* **2005**, *24*, 1181−1201.

https://doi.org/10.1021/acsami.1c01070
ACS Appl. Mater. Interfaces 2021, 13, 19244−19253